Orientation-dependent local density of states in three-dimensional photonic crystals

Jing-Feng Liu,[1,2] Hao-Xiang Jiang,[1] Chong-Jun Jin,[1] Xue-Hua Wang,[1,*] Zong-Song Gan,[3] Bao-Hua Jia,[3] and Min Gu[3,†]

[1]*State Key Laboratory of Optoelectronic Materials and Technologies, School of Physics and Engineering, Sun Yat-Sen University, Guangzhou 510275, China*

[2]*College of Science, South China Agriculture University, Guangzhou 510642, China*

[3]*Centre for Micro-Photonics and CUDOS, Faculty of Engineering and Industrial Sciences, Swinburne University of Technology, Hawthorn, Victoria 3122, Australia*

(Received 25 October 2011; published 6 January 2012)

We present a fast and efficient method to compute photonic orientation-dependent local density of states (ODLDOS) in photonic crystals (PCs) based on the point group transform of the vector field. We swiftly calculate the ODLDOS by this method and acquire the same results as that computed based on many more **k** points in half of the first Brillouin zone (FBZ) in face-center-cubic (fcc) photonic crystals. As an example, we also apply this method to investigate the properties of woodpile photonic crystals and find the remarkable differences in the ODLDOS along different polarization directions.

DOI: 10.1103/PhysRevA.85.015802 PACS number(s): 42.70.Qs, 32.80.−t, 42.50.−p

It is well known that the spontaneous emission (SE) rate of an excited quantum emitter has a strongly environmentally dependent characteristic. Control of the emission rate of quantum emitters has been demonstrated in different surrounding environments, such as microcavities [1], photonic crystals (PCs) [2–4], and metallic micro- and nanostructures [5–8]. The SE manipulation is of great importance in quantum optics, because it may limit the performance of optoelectronic devices in a diverse range of applications such as solar energy harvesting [9], light-emitting diodes [10], miniature lasers, and single-photon sources [11–13] for quantum information science.

PCs are periodic dielectric structures with variations in the refractive index on the length scale on the order of the light wavelength, which may lead to photonic band gaps [2,3]. The optical modes can be finely controlled through engineering the periodicity of the lattice, the filling ratio, and the refractive index of the PCs. As a result, since the pioneering work of Yablomovitch [2] and John [3], controlling light emission using PCs has received increasing experimental [14,15] and theoretical [16–18] attention.

The SE rate is proportional to the photonic local density of states (LDOS) [16,18,19]. Therefore, the LDOS plays a key role in the SE processes and has been extensively investigated in both theoretical simulations [19–21] and experimental probes [22]. In PCs, the LDOS can be expressed as $\rho(\omega,\mathbf{r}) = \frac{1}{(2\pi)^3}\sum_n \int_{\mathrm{FBZ}} d\mathbf{k}|\mathbf{E}_n(\mathbf{k},\mathbf{r})|^2\delta(\omega-\omega_{n\mathbf{k}})$ if the transition dipole moment of a quantum emitter is in a random orientation. Here $\omega_{n\mathbf{k}}$ and $\mathbf{E}_n(\mathbf{k},\mathbf{r})$ are respectively the frequencies and electric fields of the eigen electromagnetic modes. Its numerical simulation in PCs had been a challenging issue. Based upon the lattice-point group theory, Wang *et al.* in 2003 presented the transform method that can greatly simplify calculation of the LDOS [20]. However, the transition dipole moment of a quantum emitter is not random in many cases, such as the polarized atom, molecule and quantum dots. In these cases, the SE rate $\Gamma(\omega,\mathbf{r},\mu_{\mathbf{d}}) = \frac{\pi\omega d^2}{\varepsilon_0\hbar}\rho(\omega,\mathbf{r},\mu_{\mathbf{d}})$ [18,19] is determined by the orientation-dependent LDOS (ODLDOS) that is defined as

$$\rho(\omega,\mathbf{r},\mu_{\mathbf{d}}) = \frac{1}{(2\pi)^3}\sum_n \int_{FBZ} d\mathbf{k}|\mu_{\mathbf{d}}\cdot\mathbf{E}_n(\mathbf{k},\mathbf{r})|^2\delta(\omega-\omega_{n\mathbf{k}}), \tag{1}$$

where integration **k** vector is over the entire FBZ.

A recent experiment [23] has demonstrated that the dipole moment orientation has an important effect on SE of polarized emitters. In order to simulate the ODLDOS in Eq. (1), Nikolaev and coworkers pointed out that due to the difference of the projection results of the symmetry-related modes, inverse symmetry [21] can be applied so that the integration is not performed over the full FBZ. However, the inverse operation only reduces the integration zone to half of the full FBZ. It is still very time consuming because the eigenmodes of electromagnetic fields have to be solved in half of the full FBZ. In this paper, we develop a point group transform method, which can reduce the calculations of the ODLDOS in Eq. (1) to an irreducible Brillouin zone (IBZ) rather than to half of the full FBZ. This can significantly simplify the calculations of the ODLDOS.

Note that the FBZ is invariant under any operation of the lattice point group, and the integral in the FBZ of Eq. (1) becomes

$$\int_{\mathrm{FBZ}} d\mathbf{k}|\mu_{\mathbf{d}}\cdot\mathbf{E}_n(\mathbf{k},\mathbf{r})|^2\delta(\omega-\omega_{n\mathbf{k}}) = \int_{\mathrm{FBZ}} d\mathbf{k}|\mu_{\mathbf{d}}\cdot\mathbf{E}_n(\alpha_i[\mathbf{k}],\mathbf{r})|^2\delta(\omega-\omega_{n\alpha_i[\mathbf{k}]}), \tag{2}$$

where $\alpha_i (i = 1,2,3,\ldots,n_G)$ belongs to the corresponding crystal operation point group and $\omega_{na_i[\mathbf{k}]} = \omega_{n\mathbf{k}}$. We define an average integrating function as

$$F_n(\mathbf{k},\mathbf{r}) = \frac{1}{n_G}\sum_{a_i\in G}|\mu_{\mathbf{d}}\cdot\mathbf{E}_n(\alpha_i[\mathbf{k}],\mathbf{r})|^2, \tag{3}$$

where n_G is the number of element of point group (i.e., the number of the IBZ). From Eqs. (2) and (3), we can derive $\int_{\mathrm{FBZ}} d\mathbf{k}F_n(\mathbf{k},\mathbf{r})\delta(\omega-\omega_{n\mathbf{k}}) = \int_{\mathrm{FBZ}} d\mathbf{k}|\mu_{\mathbf{d}}\cdot\mathbf{E}_n(\mathbf{k},\mathbf{r})|^2\delta(\omega-\omega_{n\mathbf{k}})$.

*wangxueh@mail.sysu.edu.cn
†mgu@swin.edu.au

Thus, the ODLDOS can be rewritten by using the average integral function as

$$\rho(\mathbf{r},\omega,\mu_{\mathbf{d}}) = \frac{1}{(2\pi)^3}\sum_n \int_{\mathrm{FBZ}} d\mathbf{k} F_n(\mathbf{k},\mathbf{r})\delta(\omega-\omega_{n\mathbf{k}}). \quad (4)$$

Until now, the integral was not simplified because the average integrand $F_n(\mathbf{k},\mathbf{r})$ defined in Eq. (3) has to be calculated in the FBZ. We now turn to simplify the computation of the average integrand. Notice that $\mathbf{E}_n(\alpha_i[\mathbf{k}],\mathbf{r}) = \lambda_i\{\alpha_i|t\}\mathbf{E}_n(\mathbf{k},\mathbf{r})$ [20], $\{\alpha_i|t\}\mathbf{E}_n(\mathbf{k},\mathbf{r}) = \alpha_i[\mathbf{E_n}(\mathbf{k},(\alpha_i|\mathbf{t})^{-1}\mathbf{r})]$ [24], and $\alpha_i^{-1}[\mu_{\mathbf{d}}\cdot\mathbf{A}] = \alpha_i^{-1}[\mu_{\mathbf{d}}]\cdot\alpha_i^{-1}[\mathbf{A}]$ (here $|\lambda_i| = 1$, t represents the translation operator of the crystal, including the gliding operation, and $\mathbf{A}$ is a vector), so we can derive the transformation relationship between the FBZ and the real points as

$$|\mu_{\mathbf{d}}\cdot\mathbf{E}_n(\alpha_i[\mathbf{k}],\mathbf{r})|^2 = \left|\alpha_i^{-1}[\mu_{\mathbf{d}}]\cdot\mathbf{E}_n(\mathbf{k},\{\alpha_i|t\}^{-1}\mathbf{r})\right|^2. \quad (5)$$

According to Eq. (5), the average integrating function can be rewritten as

$$F_n^T(\mathbf{k},\mathbf{r}) = \frac{1}{n_G}\sum_{\alpha_i\in G}\left|\alpha_i^{-1}[\mu_{\mathbf{d}}]\cdot\mathbf{E}_n(\mathbf{k},\{\alpha_i|t\}^{-1}\mathbf{r})\right|^2. \quad (6)$$

Equation (6) means that the average integrand can be calculated in an IBZ. This means that we may solve the eigen electromagnetic fields only for a $\mathbf{k}$ point in a $\mathbf{k}$ star consisting of $\{\alpha_i[\mathbf{k}]\}$ points [20], rather than for all of different $\alpha_i[\mathbf{k}]$ points. From Eq. (3), it is easy to prove that the average integrand is invariant under any operation $\{\alpha_i\}$ of the lattice point group, that is, $F_n(\alpha_i[\mathbf{k}],\mathbf{r}) = F_n(\mathbf{k},\mathbf{r})$. Therefore, the ODLDOS can be calculated in an IBZ:

$$\rho(\mathbf{r},\omega,\mu_{\mathbf{d}}) = \frac{1}{(2\pi)^3}n_G\sum_n \int_{\mathrm{IBZ}} d\mathbf{k} F_n^T(\mathbf{k},\mathbf{r})\delta(\omega-\omega_{n\mathbf{k}}). \quad (7)$$

Equations (6) and (7) provide a very efficient and fast method to calculate the ODLDOS. Our method is $\frac{n_G}{2}$ ($n_G = 48$ for fcc structures and $n_G = 16$ for woodpile structures) times faster than the method [19,21] proposed by Koenderink *et al.* Furthermore, we can adopt the interpolation technology first proposed by Monkhorst and Pack [25] to greatly accelerate the integral calculation in Eq. (7). In general, this method can be used to effectively calculate some important physical quantities, which are related to the quantum optics and quantum information in PCs.

In the following calculations for fcc structures, the detailed numerical calculation parameters are as follows: the FBZ is divided into 16 384 coarse grids and 1 048 576 fine mesh points with the method presented by Monkhorst and Pack [25]. We first calculate the values of the $\mathbf{E}_n(\mathbf{k},\mathbf{r})$ and $\omega_{n\mathbf{k}}$ on coarse grids. Then, we explore the interpolation method to get the values of $|\mu_{\mathbf{d}}\cdot\mathbf{E}_n(\mathbf{k},\mathbf{r})|$ on the fine-mesh grids. The eigenequation is solved by an expansion of 725 plane waves.

We consider two inverse opal fcc structures presented in Ref. [21]. The first one is a TiO_2 structure, which is composed of air spheres with radius $r = 0.25\sqrt{2}a$ (here a is lattice constant). The spheres are covered by overlapping dielectric shells (refractive $\varepsilon = 6.5$) with outer radius $1.09r$, and the two adjacent spheres are connected by cylindrical vacuum windows of radius $0.4r$. In the second one, the outer radius of the overlapping dielectric Si shells is about $1.15r$ (r is the same as above) with refractive $\varepsilon = 11.9$. The radius of cylindrical vacuum windows connecting two neighboring air spheres is $0.2r$. The detail parameters and sketch of structure can be found in Ref. [21].

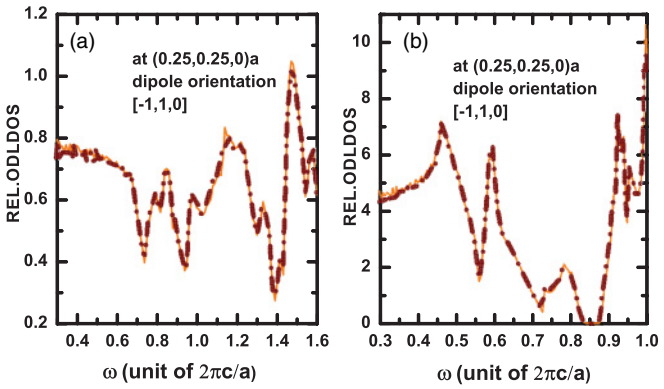

FIG. 1. (Color online) Relative ODLDOS on points $(0.25,0.25,0)a$ with a dipole orientation along $[-1,1,0]/\sqrt{2}$ in the fcc structures. The short dash-dotted maroon line and thin solid orange line correspond to our results and those in Ref. [21], respectively. (a) TiO_2 inverse opal structure with $\varepsilon = 6.5$. (b) Si inverse opal structure with $\varepsilon = 11.9$.

Based on the transform relationship (5), we exactly derived a universal Eq. (7) of the ODLDOS in PCs. We have known that the point group transformation vector t is zero in the fcc structures. Thus, the transform relationship can be rewritten as $|\alpha^{-1}[\mu_{\mathbf{d}}]\cdot\mathbf{E}_n(\mathbf{k},\alpha^{-1}\mathbf{r})|^2 = |\mu_{\mathbf{d}}\cdot\mathbf{E}_n(\alpha[\mathbf{k}],\mathbf{r})|^2$. We can easily prove through a numerical method that the transform relation is correct. To validate our point group transformation methods, we compare our results with those in Ref. [21]. We calculate the ODLDOS at point $(0.25,0.25,0)a$ of dipole orientation along the $[-1,1,0]/\sqrt{2}$ direction in two structures. The results are plotted in Fig. 1 with short dash-dotted maroon lines, and thin solid orange lines are results from Ref. [21]. The results are normalized by that in vacuum. We find that our calculation results are in good agreement with those in Ref. [21]. The deviations are very small, and this may due to the different methods in calculation structure factor, which will lead to some difference of eigenmodes and eigenfrequencies. Through comparison, we can conclude that our method is validated. However, we only select 408 $\mathbf{k}$ points in an IBZ rather than 145 708 $\mathbf{k}$ points in the half FBZ, and it takes very little time to implement the interpolation calculation. Thus, our approach makes the computation speed about $145\,708/408 \simeq 360$ times faster than that in Ref. [21]. To acquire the calculation results, we must wait about 4 days when using their method but only 15 minutes when using our method in the same computational environment.

Nowadays, many groups are interested in researching woodpile structures [13,26–30]. We now investigate the properties of the ODLDOS in woodpile structures. In this section, we consider two typical structures. The first one is designed by Lin *et al.* [26], in which the distance between four adjacent layers is denoted by c. Within each layer, the rods are separated by a distance d, where $c/d = \sqrt{2}$. The refractive index of the rods is taken as 3.60, which are placed inside the air. The width and the height of the rods are $w = 0.28d$ and $h = 0.25c$, respectively. The second is

TABLE I. $|\mu_{\mathbf{d}} \cdot \mathbf{E_n}(\mathbf{k},\mathbf{r})|^2$ for dipole orientation $\mu_{\mathbf{d}}$ and some $\mathbf{k}$, $\mathbf{r}$ points in woodpile structure.

α	$\alpha[\mathbf{k}]$	$\alpha^{-1}\mathbf{r}$	$\alpha^{-1}[\mu_{\mathbf{d}}]/\sqrt{14}$	$\mathbf{E}_1^{\alpha\mathbf{k}}$	$\mathbf{E}_1^{\alpha\mathbf{r}\mu}$	$\mathbf{E}_2^{\alpha\mathbf{k}}$	$\mathbf{E}_2^{\alpha\mathbf{r}\mu}$	$\mathbf{E}_3^{\alpha\mathbf{k}}$	$\mathbf{E}_3^{\alpha\mathbf{r}\mu}$
$(E\|0)$	(0.8,0.4,0.2)	(0.2,0.1,0.05)	(1.0,2.0,3.0)	0.0001	0.0001	0.0584	0.0584	0.0343	0.0343
$(c_{2z}\|0)$	(−0.8, −0.4,0.2)	(−0.1, −0.05, −0.2)	(−1.0, −2.0,3.0)	0.0008	0.0008	0.0476	0.0476	0.2632	0.2632
$(c_{2x}\|0)$	(0.8, −0.4, −0.2)	(−0.15, −0.2, −0.2)	(1.0, −2.0, −3.0)	0.0123	0.0123	0.0186	0.0186	0.0453	0.0453
$(c_{2y}\|0)$	(−0.8,0.4, −0.2)	(−0.45, −0.35,0.05)	(−1.0,2.0, −3.0)	0.0549	0.0549	0.0273	0.0273	0.0010	0.0010
$(Ic_{4z}\|0)$	(−0.4,0.8, −0.2)	(−0.45,0.1, −0.3)	(2.0, −1.0, −3.0)	0.0310	0.0310	0.0103	0.0103	0.0078	0.0078
$(Ic_{4z}^{-1}\|0)$	(0.4, −0.8, −0.2)	(−0.15, −0.05, −0.05)	(−2.0,1.0, −3.0)	0.0281	0.0281	0.0548	0.0548	0.1379	0.1379
$(Ic_{2xy}\|0)$	(−0.4, −0.8,0.2)	(0.2, −0.35, −0.3)	(−2.0, −1.0,3.0)	0.0002	0.0002	0.0313	0.0313	0.2768	0.2768
$(Ic_{2x\bar{y}}\|0)$	(0.4,0.8,0.2)	(−0.1, −0.2, −0.05)	(2.0,1.0,3.0)	0.0093	0.0093	0.0481	0.0481	0.0145	0.0145
$(I\|\tau)$	(−0.8, −0.4, −0.2)	(−0.2, −0.1, −0.05)	(−1.0, −2.0, −3.0)	0.0001	0.0001	0.0584	0.0582	0.0343	0.0343
$(c_{4z}\|\tau)$	(0.4, −0.8,0.2)	(0.1, −0.45, −0.3)	(−2.0,1.0,3.0)	0.0008	0.0008	0.0476	0.0476	0.2632	0.2632
$(c_{4z}^{-1}\|\tau)$	(−0.4,0.8,0.2)	(−0.35,0.2, −0.3)	(2.0, −1.0,3.0)	0.0123	0.0123	0.0186	0.0186	0.0453	0.0453
$(c_{2xy}\|\tau)$	(0.4,0.8, −0.2)	(−0.05, −0.15, −0.05)	(2.0,1.0, −3.0)	0.0549	0.0549	0.0273	0.0273	0.0010	0.0010
$(c_{2x\bar{y}}\|\tau)$	(−0.4, −0.8, −0.2)	(−0.05, −0.1, −0.2)	(−2.0, −1.0, −3.0)	0.0310	0.0310	0.0103	0.0103	0.0078	0.0078
$(Ic_{2z}\|\tau)$	(0.8,0.4, −0.2)	(−0.35, −0.45,0.05)	(1.0,2.0, −3.0)	0.0281	0.0281	0.0548	0.0548	0.1379	0.1379
$(Ic_{2x}\|\tau)$	(−0.8,0.4,0.2)	(−0.2, −0.15, −0.2)	(−1.0,2.0,3.0)	0.0002	0.0002	0.0313	0.0313	0.2768	0.2768
$(Ic_{2y}\|\tau)$	(0.8, −0.4,0.2)	(0.1,0.2,0.05)	(1.0, −2.0,3.0)	0.0093	0.0093	0.0481	0.0481	0.0145	0.0145

a germanium inverse woodpile structure [28]. We adopt the experimental parameters given in that article. In the following calculations, the FBZ is also divided into 16 384 coarse grids and 1 048 576 fine mesh points, and the method is the same as that in the fcc structures. Through detailed analysis, the lattice of the woodpile structures belongs to the diamond lattice group. In the diamond lattice with a global basis, the point group corresponds to the O_h^7 group. However, in the woodpile structure, the basis is composed of three rods, which has lower operation symmetry than the globule. Thus, other than 48-fold symmetry operations, there are only 16-fold symmetry operations are as follows: $\{E|0\}$, $\{c_{2z}|0\}$, $\{c_{2x}|0\}$, $\{c_{2y}|0\}$, $\{Ic_{4z}|0\}$, $\{Ic_{4z}^{-1}|0\}$, $\{Ic_{2xy}|0\}$, $\{Ic_{2x\bar{y}}|0\}$, $\{I|\tau\}$, $\{c_{4z}|\tau\}$, $\{c_{4z}^{-1}|\tau\}$, $\{c_{2xy}|\tau\}$, $\{c_{2x\bar{y}}|\tau\}$, $\{Ic_{2z}|\tau\}$, $\{Ic_{2x}|\tau\}$, and $\{Ic_{2y}|\tau\}$. As a result, the IBZ for a woodpile structure is different from those for diamond and fcc structures. In an IBZ, there are 1088 $\mathbf{k}$ points in the woodpile structures and 408 $\mathbf{k}$ points in the diamond and fcc structures. In order to acquire ODLDOS of the woodpile structures, we adopt similar methods and process as in the fcc structures.

The transform relationship in Eq. (5) in a germanium inverse woodpile structure [28] for some $\mathbf{k}$ points and real-space $\mathbf{r}$ points are shown in Table I, in which Schoenflies notations are adopted to describe the lattice point group. The $\mathbf{k}$ points belong to a $\mathbf{k}$ star, and all operations of the star are given here for the sake of detailed comparison of the results of the transform relation. Without loss of generality, we randomly select a dipole orientation $\mu_{\mathbf{d}} = (1,2,3)/\sqrt{14}$. For convenience, we use $\mathbf{E}_n^{\alpha\mathbf{k}}$ and $\mathbf{E}_n^{\alpha\mathbf{r}\mu}$ to denote $|\mu_{\mathbf{d}} \cdot \mathbf{E}_n(\alpha[\mathbf{k}],\mathbf{r})|^2$ and $|\alpha^{-1}\mu_{\mathbf{d}} \cdot \mathbf{E}_n(\mathbf{k},(\alpha|t)^{-1}\mathbf{r})|^2$ in Table I, respectively. Thus, we can clearly see that the values of $|\alpha^{-1}\mu_{\mathbf{d}} \cdot \mathbf{E}_n(\mathbf{k},(\alpha|t)^{-1}\mathbf{r})|^2$ are always equal to those of $|\mu_{\mathbf{d}} \cdot \mathbf{E}_n(\alpha[\mathbf{k}],\mathbf{r})|^2$. This proves that our methods are also valid in woodpile structures.

Figure 2(a) shows the relative ODLDOS and the surface of relative ODLDOS at point $(0.275,0.275,-0.135)a$ in the first woodpile structure. The relative results are normalized in the vacuum. We can see that the ODLDOS is highly anisotropic since it is very different for the three orientations. In general, the ODLDOS is highest for the $\mu_{\mathbf{d}} = [0,0,1]$ orientation, intermediate for $\mu_{\mathbf{d}} = [-1,1,0]/\sqrt{2}$ orientation, and lowest for the $\mu_{\mathbf{d}} = [1,1,0]/\sqrt{2}$ orientation. Furthermore, we plot the surface of the ODLDOS in a subplot in Fig. 2(a). The surfaces of the ODLDOS are calculated according to the method presented by Vos and coworkers [19]. For convenience, we choose the reduced transition frequency $\omega = 0.604$ in the subplot. The surface is double-sphere-like, and the anisotropy $(\rho_{\max}/\rho_{\min})$ is 12.8. We find the maximal ODLDOS 15.37 for the $\mu_{\mathbf{d}} = [-0.415,0.572,0.707]$ orientation. Figure 2(b) shows the relative ODLDOS and the surface of relative ODLDOS at point $(0,0,0.25)a$ in the second woodpile structure. The three dipole orientations are the same as those in Fig. 2(a). However, the ODLDOS is highest for the $\mu_{\mathbf{d}} = [1,1,0]$ orientation, which is different from Fig. 2(a). If the reduced transition frequencies

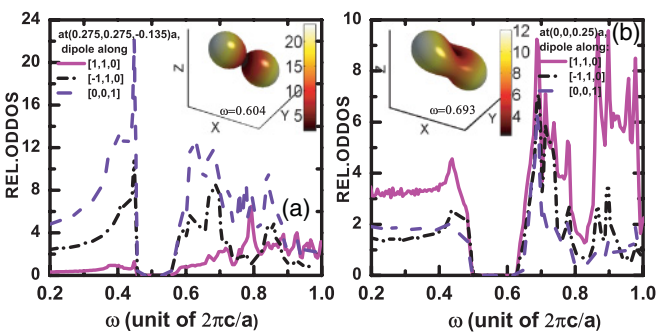

FIG. 2. (Color online) The relative ODLDOS and the surface of the relative ODLDOS in the woodpile structures. (a) In the first woodpile structure at point $(0.275,0.275,-0.135)a$, the ODLDOS along the [1,1,0], [−1,1,0] and [0,0,1] directions are shown by the solid maroon, short dash-dotted black, and dashed violet curves, respectively. The subplot gives the surface of the ODLDOS at a reduced frequency 0.604. (b) In the second woodpile structure at point $(0,0,0.25)a$, the ODLDOS along the [1,1,0], [−1,1,0], and [0, 0,1] directions are shown by the solid maroon, short dash-dotted black, and dashed violet curves, respectively. The subplot gives the surface of the ODLDOS at a reduced frequency, 0.693.

are below 0.69, the two other dipole orientations have small differences in the ODLDOS, and if the transition frequencies are higher than 0.69, the ODLDOS along the [−1,1,0] direction are higher. In the subplot of Fig. 2(b), we present the surface of ODLDOS at a reduced transition frequency 0.693. The anisotropy ($\rho_{\max}/\rho_{\min}$) is 5.5. Figure 2 gives an intuitive picture of the orientation-dependent behavior. We know that the SE rate is proportional to the ODLDOS [18,19]. Therefore, the control of the polarization direction is conducive to strong emission enhancement. Our methods can quickly scan points with the higher ODLDOS, which may lead strong quantum electrodynamics effects beyond the weak coupling condition.

In summary, we have theoretically and numerically studied a transform relationship of electric fields in PCs between reciprocal **k** points and real-space **r** points under a lattice point group operation. Based on this transformation, we have derived an averaged integral function for calculating the ODLDOS and the surface of the ODLDOS. Using this integrand, the computing time can be dramatically reduced. The validity of our method is also proved. It is found that the ODLDOS will greatly change along different orientations. This provides an effective way to control the SE of the quantum emitters.

We acknowledge the financial support from the Chinese National Key Basic Research Special Fund (Grants No. 2006CB921706 and No. 2010CB923200) and the National Natural Science Foundation of China (Grants No. 10725420, No. 11104083, and No. U0934002). This research was partly conducted by the Australian Research Council Centre of Excellence for Ultrahigh Bandwidth Devices for Optical Systems (Project No. CE110001018). Baohua Jia is supported by the Australian Research Council (Project No. DP0987006).

[1] K. J. Vahala, Nature (London) **424**, 839 (2003).
[2] E. Yablonovitch, Phys. Rev. Lett. **58**, 2059 (1987).
[3] S. John, Phys. Rev. Lett. **58**, 2486 (1987).
[4] S. Noda *et al.*, Nat. Photon. **1**, 449 (2007).
[5] D. E. Chang, A. S. Sorensen, P. R. Hemmer, and M. D. Lukin, Phys. Rev. Lett. **97**, 053002 (2006).
[6] A. V. Akimov *et al.*, Nature (London) **450**, 402 (2007).
[7] G.-Y. Chen *et al.*, Opt. Lett. **33**, 2212 (2008).
[8] A. F. Koenderink, Nano Lett. **9**, 4228 (2009).
[9] M. Gratzel, Nature (London) **414**, 338 (2001).
[10] J. J. Wierer *et al.*, Nat. Photon. **3**, 163 (2009).
[11] C. Santori, M. Pelton, G. Solomon, Y. Dale, and Y. Yamamoto, Phys. Rev. Lett. **86**, 1502 (2001); W.-H. Chang *et al.*, *ibid.* **96**, 117401 (2006).
[12] S. Strauf *et al.*, Nat. Photon. **1**, 704 (2007).
[13] A. Tandaechanurat *et al.*, Nat. Photon. **5**, 91 (2011).
[14] E. P. Petrov, V. N. Bogomolov, I. I. Kalosha, and S. V. Gaponenko, Phys. Rev. Lett. **81**, 77 (1998); M. Megens, J. E. G. J. Wijnhoven, A. Lagendijk, and W. L. Vos, Phys. Rev. A **59**, 4727 (1999).
[15] P. Lodahl *et al.*, Nature (London) **430**, 654 (2004); K. Hennessy *et al.*, *ibid.* **445**, 896 (2007).
[16] R. Sprik *et al.*, Europhys. Lett. **35**, 265 (1996); K. Busch and S. John, Phys. Rev. E **58**, 3896 (1998).
[17] S. John and J. Wang, Phys. Rev. Lett. **64**, 2418 (1990); S. Y. Zhu, Y. Yang, H. Chen, H. Zheng, and M. S. Zubairy, *ibid.* **84**, 2136 (2000); Z. Y. Li, L. L. Lin, and Z. Q. Zhang, *ibid.* **84**, 4341 (2000).
[18] Y. S. Zhou, X. H. Wang, B. Y. Gu, and F. H. Wang, Phys. Rev. Lett. **96**, 103601 (2006).
[19] W. L. Vos, A. F. Koenderink, and I. S. Nikolaev, Phys. Rev. A **80**, 053802 (2009).
[20] R. Wang, X. H. Wang, B. Y. Gu, and G. Z. Yang, Phys. Rev. B **67**, 155114 (2003).
[21] I. S. Nikolaev, W. L. Vos, and A. F. Koenderink, J. Opt. Soc. Am. B **26**, 987 (2009).
[22] Q. Wang, S. Stobbe, and P. Lodahl, Phys. Rev. Lett. **107**, 167404 (2011); M. Frimmer, Y. Chen, and A. F. Koenderink, *ibid.* **107**, 123602 (2011); M. D. Birowosuto, S. E. Skipetrov, W. L. Vos, and A. P. Mosk, *ibid.* **105**, 013904 (2010); V. Krachmalnicoff, E. Castanie, Y. DeWilde, and R. Carminati, *ibid.* **105**, 183901 (2010).
[23] Q. Wang *et al.*, Opt. Lett. **35**, 2768 (2010).
[24] K. Sakoda, *Optical Properties of Photonic Crystals* (Springer, Berlin, 2005).
[25] H. J. Monkhorst and J. D. Pack, Phys. Rev. B **13**, 5188 (1976).
[26] S. Y. Lin *et al.*, Nature (London) **394**, 251 (1998).
[27] K. Aoki *et al.*, Nat. Mater. **2**, 117 (2003); G. M. Gratson *et al.*, Adv. Mater. **18**, 461 (2006).
[28] F. Garca-Santamara *et al.*, Adv. Mater. **19**, 1567 (2007).
[29] S. Takahashi *et al.*, Nat. Mater. **8**, 721 (2009).
[30] J. Li *et al.*, Adv. Mater. **19**, 3276 (2007); M. J. Ventura *et al.*, *ibid.* **20**, 1329 (2008); M. Gu *et al.*, Laser Photon. Rev. **4**, 414 (2010).